# Relativistic Description of Nucleon-Nucleon Interaction Using a Complex Potential

T. Ueda,* M. L. Nack, and A. E. S. Green
*Department of Physics and Astronomy, University of Florida, Gainesville, Florida 32601*

(Received 6 July 1973)

Using a three-dimensional reduction of the Bethe-Salpeter equation, we calculate the nucleon-nucleon phase parameters in the energy range of 0–1 GeV of incident laboratory energy. In the elastic energy region the generalized one-boson-exchange potential is assumed for driving terms and in the inelastic energy region an imaginary potential is added. Ingredients of the one-boson-exchange potential are $\pi$, $\rho$, $\omega$, $\eta$, $\delta$, and $S^*$ mesons. The dipole form factor is adopted for all the interactions of mesons with nucleons. The broad mass distribution is also taken into account for the $\rho$ and $S^*$ resonances. Our imaginary potential which is given by a superposition of regularized Yukawa potentials which have an attractive long-range part and a repulsive core, can describe the peripheral nature of the absorption found in phase-shift analyses. Comparisons of our theoretical phase shifts with those derived by the phase-shift analyses, and of our theoretical observables with experiments at 660 and 970 MeV are made in detail and physical implications are discusssed.

[NUCLEAR REACTIONS $N$-$N$ interaction, 0–1000 MeV; calculated phase parameters, observables.]

## 1. INTRODUCTION

For the past decade it has been shown that the $N$-$N$ interaction in the elastic energy region can be well described in terms of the one-boson-exchange model.[1] An early finding of the validity of the model in the intermediate region of the nuclear force[2] and subsequent development with introduction of the form factor by Ueda and Green,[3] or the regularization by Green and Sawada[4] founded on the generalized meson theory of Green[5] permitted the model to describe the whole elastic $N$-$N$ data very successfully. Furthermore Gersten, Thompson, and Green presented a relativistic version of the generalized one-boson-exchange potential,[6] using a three-dimensional reduction of the Bethe-Salpeter (BS) equation.[7] (This work will be referred to as GTG.)

With such a background it would appear worthwhile to attempt to extend this relativistic version of the model to the inelastic energy region. Thus, a $K$-matrix unitarization method[8,9] and a dispersion-relation calculation[10] have been applied by Ueda to the 0–1-GeV region. In these works inelastic effects are treated within a framework of the one-boson-exchange model and a good description of the elastic $N$-$N$ data is achieved.

In this paper we extend the GTG approach to the inelastic energy region up to 1 GeV by utilizing a complex potential. In the GTG treatment the BS equation is solved in momentum space with a relativistic two-nucleon propagator derived by Thompson[11] in which the two nucleons are in a positive energy state and the relative energy part is equal to zero. The same propagator is used also in this work. The real part of our potential is the generalized one-boson-exchange potential (OBEP) whose ingredients are $\pi$, $\eta$, $\rho$, $\omega$, $S^*$, and $\delta$ mesons interacting with nucleons having a dipole form factor. We allow for the broad mass distributions of the $\rho$ and $S^*$ resonances with the help of representations recently obtained by Nack, Ueda, and Green.[12]

In the inelastic energy region we add a phenomenological imaginary potential which (in configuration space language) consists of a long-range attractive-regularized Yukawa potential and a short-range repulsive-regularized Yukawa potential. The spin dependence of the imaginary potential is assumed to be $L=0$ and even-parity exchange type, i.e., analogous to scalar meson exchange. With this phenomenological augmentation we achieve a satisfactory description of the $N$-$N$ data in the 0–1-GeV energy range.

## 2. FORMALISM

Our three-dimensional equation with the complex potential can be derived from the original Bethe-Salpeter equation with a complex interaction kernel by an analogous procedure to that worked out by Thompson[11] for the elastic case. We obtain (suppressing spin indices)

$$K(\vec{p},\vec{k}) = V(\vec{p},\vec{k}) + \int_0^\infty \vec{q}^2\, d\vec{q}\, V(\vec{p},\vec{q}) G(\vec{q},\vec{k}) K(\vec{q},\vec{k}), \quad (1)$$

where $\vec{p}$ and $\vec{k}$ are the final and initial c.m. momentum of the scattered nucleon, respectively, and $V(\vec{p},\vec{q})$ is now a complex potential,

$$V(\vec{p},\vec{q}) = V_R(\vec{p},\vec{q}) + iV_I(\vec{p},\vec{q}). \quad (2)$$

$G(\vec{q},\vec{k})$ is a two-nucleon propagator given by

$$G(\vec{q},\vec{k}) = P\{4\pi^3 m^2/E^2(\vec{q})[E(\vec{q}) - E(\vec{k})]\}, \quad (3)$$

where $E(\vec{k}) = (\vec{k}^2 + m^2)^{1/2}$, $m$ is the nucleon mass, and $P$ denotes the principal value. This propagator can be derived by considering only contributions of two intermediate nucleons which are in positive energy states and have zero relative energy.

$K(\vec{p}, \vec{k})$ which is determined by Eq. (1) is obviously a complex quantity and related to the $S$ matrix in an operator form by means of

$$S = \frac{1 + iK/\pi\rho}{1 - iK/\pi\rho}, \tag{4}$$

where $\rho = E(\vec{k})/k$.

The real part $V_R$ of the complex potential is assumed to be the generalized one-boson-exchange potential, or the one-boson-exchange potential modified by the form factor. For the pseudoscalar, scalar, and vector meson, respectively, they are derived from the interaction Hamiltonian densities,

$$\begin{aligned} H_{ps} &= F(\vec{k}^2)\, g_{ps}\bar{\psi}(\vec{p}) i\gamma_5 \psi(\vec{q})\phi_{ps}(\vec{k}), \\ H_s &= F(\vec{k}^2)\, g_s \bar{\psi}(\vec{p})\psi(\vec{q})\phi_s(\vec{k}), \\ H_v &= F(\vec{k}^2)\left\{ g_v \bar{\psi}(\vec{p}) i\gamma_\mu \psi(\vec{q})\phi_\mu^v(\vec{k}) \right. \\ &\quad \left. + i\frac{fv}{2m}\bar{\psi}(\vec{p})\sigma_{\mu\nu}\psi(\vec{q})[k_\mu \phi_\nu^v(\vec{k}) - k_\nu \phi_\mu^v(\vec{k})] \right\}, \end{aligned} \tag{5}$$

where $\vec{k} = \vec{p} - \vec{q}$, $\sigma_{\mu\nu} = (\gamma_\mu\gamma_\nu - \gamma_\nu\gamma_\mu)/2i$, and

$$F(\vec{k}^2) = \left(\frac{\Lambda^2}{\vec{k} + \Lambda^2}\right)^2. \tag{6}$$

The imaginary part $V_I$ of the complex potential is assumed to be $L = 0$ and an even-parity exchange type given by

$$\begin{aligned} V_I(\vec{p}, \vec{q}) &= \bar{\omega}(\vec{q})\omega(\vec{k})\bar{\omega}(-\vec{q})\omega(-\vec{k}) \\ &\quad \times [v_0(\vec{q}, \vec{k}) + \vec{\tau}_1 \cdot \vec{\tau}_2 v_1(\vec{q}, \vec{k})], \end{aligned} \tag{7}$$

where $\omega$'s are the Dirac spinors whose explicit definition is given in Ref. 11. $v_0$ and $v_1$ represent components of $I = 0$ and $I = 1$ exchange, respectively, and are independent of the spin state. We parametrize these functions using

$$\begin{aligned} v_i(\vec{q}, \vec{k}) &= \frac{(g_l^i)^2}{\Lambda_l^2}\left(\frac{1}{1 + (\vec{q} - \vec{k})^2/\Lambda_l^2}\right)^5 \\ &\quad - \frac{(g_h^i)^2}{\Lambda_h^2}\left(\frac{1}{1 + (\vec{q} - \vec{k})^2/\Lambda_h^2}\right)^5. \end{aligned} \tag{8}$$

By choosing $\Lambda_l < \Lambda_h$, we achieve a shape which characterizes the peripheral nature of the absorption. In calculations for the 0–450-MeV energy range this imaginary potential is deleted. However, it is included in calculations at 660 and 970 MeV where inelastic effects are important and its parameters are adjusted at both energies. In the actual calculation the factor of $[F(\vec{k}^2)]^2$ from Eq. (6), appearing in $V_R$ from using Eq. (5) and in $V_I$ from using Eq. (8), is replaced by $\Pi_{i=1}^{n}[\Lambda_i^2/(\vec{k}^2 + \Lambda_i^2)]$, where $\Lambda_i = [1 + (i-1)/100]\Lambda$ and $n = (4, 5)$ for $(V_R, V_I)$, respectively.

Partial-wave expansions of the component one-boson-exchange potentials have been given by Ueda[2,10] for the on-mass-shell case and by GTG[6] for off-mass-shell cases. Since the partial-wave expansion of the imaginary potential parametrized by Eq. (8) may be obtained from similar formulas as the real potential, we will not repeat them here.

The $S$ matrix given by Eq. (4) is expanded into partial wave components and in the case of spin-uncoupled scattering it is represented by

$$S_J = r_J e^{2i\delta_J}, \tag{9}$$

where $\delta_J$ and $r_J$ are a real phase shift and a reflection parameter associated with a partial wave of total angular momentum $J$. The corresponding representation for spin-coupled scattering and a relation of $r_J$ to the inelastic cross section are given in the Appendix.

## 3. MODEL PARAMETERS

The ingredients of the real potential are $\pi$, $\rho$, $\omega$, $\eta$, $\delta$, and $S^*$ mesons. The masses of $\pi$, $\omega$, $\eta$, and $\delta$ are fixed at the experimentally observed resonance values. Special attention, however, is given to the $\rho$ and $S^*$ mass distributions. The mass of the $\rho$ is taken as 840 MeV with zero width which is approximately equivalent in effect to the actual $\rho$ contribution with the mass distribution.[12] The $I = 0$ $S$-wave phase shfit of the $\pi$-$\pi$ scattering shows a broad mass distribution of the $\pi$-$\pi$ system. The present data have some ambiguity in the 700–1000-MeV region, however, we adopt the $S^*$ solution which seems at this time to have the most experimental support. We represent the effect of the broad mass distribution of the $S^*$ solution by two $I = 0$ scalar mesons $\sigma_l$ and $\sigma_h$.[12] These, in effect, correspond to $\sigma$ and $\eta_v$ in the Ueda-Green I model.[3] However, in this case the masses of $\sigma_l$ and $\sigma_h$ are constrained to be consistent with the $S^*$ solution. The form-factor parameter $\Lambda$ is taken in common for all mesons. Adjustable parameters are $m(\sigma_l)$, the coupling constants and the form-factor parameter $\Lambda$. As in our previous works we assumed simply $(f/g)_\omega = 0$ in accord with the isoscalar part of the electromagnetic form factor. However, a small value for this ratio can be allowed as used in a recent work by Ueda,[13] Furuichi, Suemitsu, Yonezawa, and Watari,[14] and Bryan and Gersten.[15] The coupling constants and $\Lambda$ are adjusted so as to secure fits to the Livermore phase shifts (the energy-independent solution) at 25, 50, 95, 142, 210, and 330 MeV.[16]

After determining the real potential the parameters of the imaginary potential are adjusted to achieve a fit to the reflection parameters of *pp* scattering obtained by the phase-shift analyses[17] or by some theoretical models,[8,9,18] and also to yield the inelastic cross sections of *pp* and *np* scattering at 660 and 970 MeV. As seen in Eq. (8) the imaginary potential has a set of parameters of $g_l^0$, $g_h^0$; $g_l^1$, $g_h^1$; $\Lambda_l$, $\Lambda_h$. We determined $\Lambda_l$ and $\Lambda_h$ by using the pheripheral-type-reflection parameters and took them in common at 660 and 970 MeV. $g_l^0$, $g_h^0$; $g_l^1$ and $g_h^1$ are chosen to yield fits to the *pp* and *np* inelastic cross sections as well as the reflection parameters. Care has been taken not to violate the unitarity limit, since too large a value for the repulsive part would create such a problem.

## 4. DATA FOR COMPARISONS

For experimental data we use the phase parameters obtained by the Livermore group through energy-independent analyses at 25, 50, 95, 142, 210, 330, 425, and 630 MeV.[16] For the $\epsilon_1$ parameter which has a large ambiguity in the phase-shift analysis solutions we also take the energy-dependent solution of the Livermore group obtained in the 0–750-MeV energy range. Comparisons are also made with the Yale phase parameters in the 0–350-MeV energy range.[19] At 660 MeV we use phase parameters obtained by the Kyoto group,[17a] and at 970 MeV we take those obtained by the Kyoto group,[17] although error bars are not available at this energy.

The reflection parameters to be compared with our theoretical results are of two kinds. The first ones are those obtained by the phase-shift analyses of *pp* scattering at 660 and 970 MeV by the Kyoto group.[17] In their analyses at 660-MeV peripheral absorption is assumed according to the Mandelstam model.[20] Thus the $^1S_0$ reflection parameter is fixed to unity and the reflection parameters of *P*, *D*, and *F* waves were searched as well as the real phase shifts to make a fit to the elastic and inelastic cross sections. At 970 MeV too, similar analyses as well as analyses not constrained by the Mandelstam model have been presented. The latter are predictions of theoretical models. Amaldi[18] calculated reflection parameters in the 600–1400-MeV energy range, using the one-pion-exchange model modified by the form factor for the one-pion production process which is dominant in the inelastic processes of the energy range. The *K*-matrix unitarization model given by Ueda and others also provides the reflection parameters.[8,9] In this model the one-boson-exchange amplitudes for *pp* scattering and $pp \to NN^*$ reaction are simultaneously unitarized by the damping relation and the reflection parameters are obtained by fitting the model to both elastic and inelastic data. Unfortunately, the reflection parameters obtained by these various methods show considerable ambiguities at 660 and 970 MeV.

Inelastic cross sections were evaluated from experimental total cross sections and elastic total cross sections at 660 and 970 MeV, except for the *pn* inelastic cross section at 660 MeV.[21–26] To obtain the *pn* inelastic cross section at 660 MeV, we used a value derived by integrating the elastic differential cross section at 660 MeV.

The data for the *pp* and *np* observables, as defined in the review article by Hoshizaki,[27] are taken from the *NN* scattering data compilation by Bystricky, Lehar, and Janout at Saclay (1972).[28] We use their tabulated data which are at times only graphically represented in the 34 original articles cited under Ref. 28 using their reference code.

## 5. NUMERICAL RESULTS AND COMPARISON WITH DATA

Numerical results of the phase parameters and reflection coefficients and inelastic cross sections are shown in Figs. 1 and 2, and in Tables I–IV.

### A. Real Phase Parameters

We present two solutions of our search procedure for the real potential. The No. 1 solution resembles the U-G model of Ref. 3 in each contribution of its ingredients, and solution No. 2 resembles the GTG model. The $\chi^2$ test per 103 phase parameters with $J \leq 5$, using the Livermore energy-independent solution[16] at 25, 50, 95, 142, 210, and 330 MeV, produced results of 4.5 and 3.9 for the No. 1 and 2 solutions, respectively. Thus, the No. 2 solution gives a little better fit in the elastic energy region, and the No. 1 solution gives better fits in $^1D_2$ and $\epsilon_1$ at 660 and 970 MeV and also has $(f/g)_\rho = 4.96$, which is nearer the electromagnetic form-factor value of $(f/g)_\rho \approx 4$ than No. 2.

At 660 MeV the phase-shift analysis solutions have large error bars. Our result for the 12 phase parameters shows that deviations are less than about 3 standard deviation except for the $^3D_1$ phase shift. The phase-shift analyses give considerable ambiguity for the $\epsilon_1$ parameter at this energy. In particular it is noted that the energy-dependent analyses yield values of opposite sign from those of energy-independent analyses. Our theoretical prediction is nearer to the energy-dependent results.

At 970 MeV the phase-shift analyses by the Kyoto group give two sets of solutions for *pp* scattering

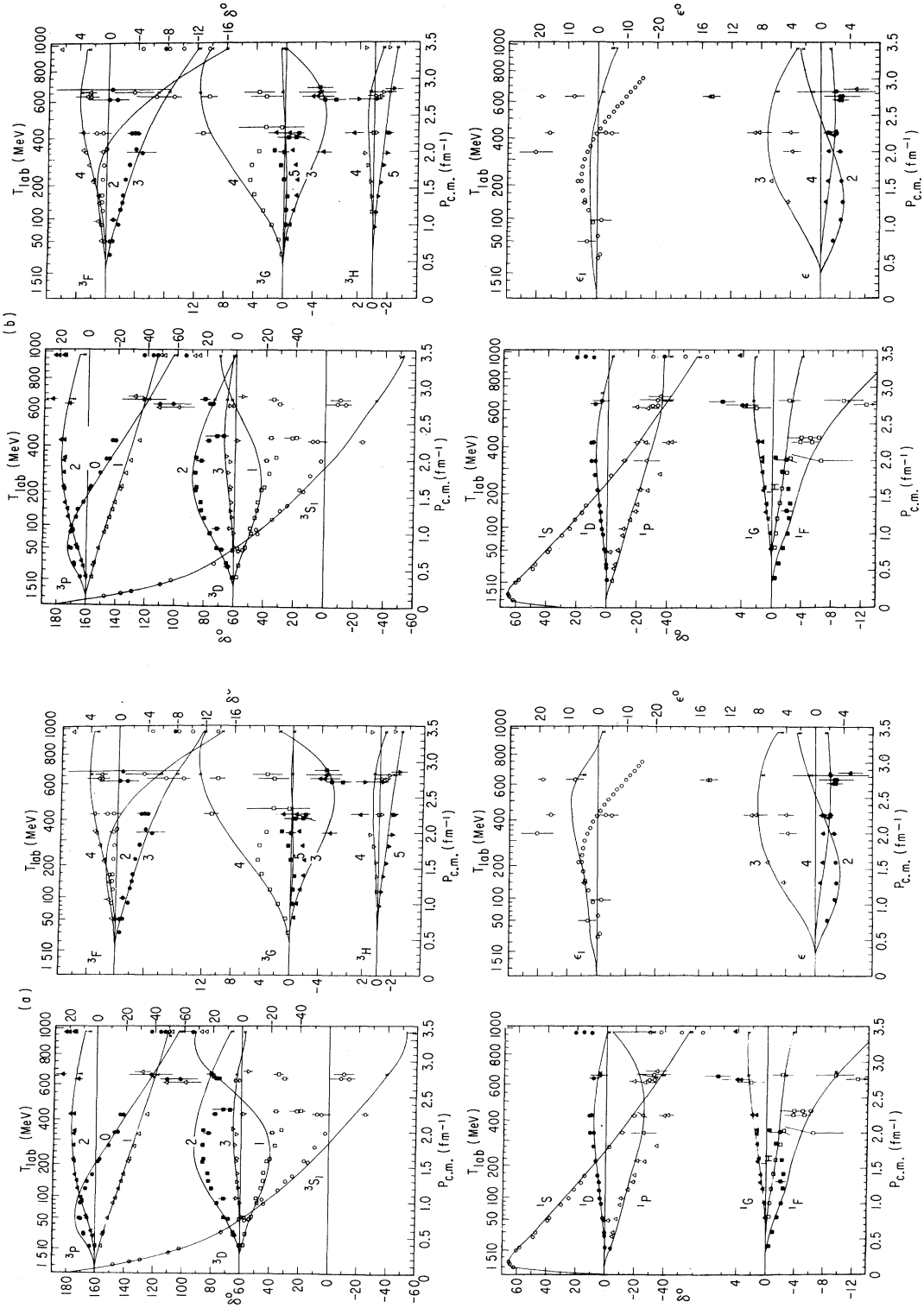

FIG. 1. Fits of our 16-parameter solutions to the $N$-$N$ phase-shift data over $T_{\mathrm{lab}} = 0$, 970 MeV for (a) solution 1, and (b) solution 2. The points of the smooth curves are generated by the 10-parameter real potential. The addition of the six- (energy-dependent) parameter imaginary potential at 660 and 970 MeV is denoted by crosses with connecting lines to the smooth curves illustrating the shift of the smooth curves due to the introduction of the imaginary potential.

phase parameters and no error bar is available. Our theoretical values of the six phase parameters for the $pp$ scattering are consistent qualitatively with those of the phase-shift analyses, except in the case of the $^1D_2$ state where a rather large difference develops.

### B. Low-Energy and Deuteron Parameters

We constrained our solutions to fit the $(n, p)$ energy-dependent phase shifts, $^1S_0$ and $^3S_1$, of Table VII of Ref. 16 at 1, 2, 3, and 10 MeV. Using effective range theory[29,30] the singlet and triplet scattering lengths $(a_s, a_t)$ and the effective ranges $(r_s, r_t)$ are calculated by using

$$k\cot\delta = -\frac{1}{a} + \tfrac{1}{2} rk^2 + O(k^4)$$

at 1 and 2 MeV, where $k$ is the c.m. momentum of the nucleon of mass $m$. The minus root of the related quadratic equation

$$\gamma = (mE_d)^{1/2}/\hbar c = \frac{1}{a_t} + \tfrac{1}{2} r_t\gamma^2$$

gives the deuteron radius $\gamma^{-1}$ and binding energy $E_d$. The quadrupole moment of the deuteron $Q$ is obtained at 2 MeV using our values of $r_t$ and $\gamma$, and

$$\tan\epsilon_1 = [\sqrt{2}\,(1-\gamma r_t)Q]k^2 + O(k^4)\,.$$

The values of $a_s$, $r_s$, $a_t$, $r_t$, $E_d$, and $Q$ are shown in Table V as determined by $\delta(^1S_0)$, $\delta(^3S_1)$, and $\epsilon_1$ of Ref. 16 and our solutions 1 and 2, and they can be compared with the experimental values. A better experimental determination of the low-energy behavior of $\epsilon_1$ is necessary for an improved prediction of $Q$ from these values as $k^2 \to 0$, and for a means of properly constraining theoretical calculations of $\epsilon_1$ for $k^2 \to 0$. A more direct method of examining the nonrelativistic deuteron low-energy parameters for generalized OBEP models has been given by Gersten and Green.[31]

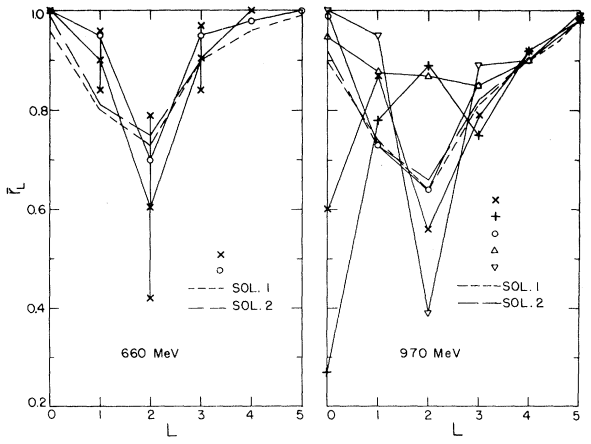


FIG. 2. The $pp$ reflection parameters $\bar{r}_L$ of fixed $L$ averaged over $J$ at 660 and 970 MeV, where $\bar{r}_L = N^{-1} \times \sum_{i=1}^{N} r_{L J_i}$. The solid lines go through past phase-shift analyses [Ref. 17a (cross) at 660 MeV, and Ref. 17b (cross and plus at 970 MeV)] and also past-averaged theoretical predictions [Ref. 8 (up-triangle), Ref. 9 (down-triangle), and Ref. 18 (circle)], and the dashed (sol. 1) and broken (sol. 2) lines go through our theoretical predictions. Only one dashed curve indicates our solutions coincide at these points.

TABLE I. Parameters of the generalized OBEP.

| Meson | Mass (MeV) | No. 1 $g^2$ | No. 2 $g^2$ |
|---|---|---|---|
| $\pi$ | 138.7 | 14.600 | 14.200 |
| $\delta$ | 960.0 | 1.345 | 0.369 |
| $\rho$ | 840.0 | 0.751 | 0.500 |
| $(f/g)_\rho$ | | 4.963 | 6.376 |
| $\omega$ | 782.8 | 8.800 | 9.917 |
| $\sigma_h$ | 790.0 | 8.814 | 10.960 |
| $\sigma_l$ | 352.0 | 0.738 | 0.700 |
| $\eta$ | 548.8 | 2.486 | 3.091 |
| $\Lambda$(MeV) | | 2075.0 | 1860.0 |
| $\chi^2$/data | | 4.5 | 3.9 |

### C. Imaginary Phase Parameters or Reflection Parameters

At 660 MeV our imaginary potential gives quantitative agreements with the experimental values of the inelastic cross sections of both of $pp$ and $np$ scattering. In addition the peripheral nature of the absorption is consistent with results of the phase-shift analyses or the predictions of theoretical models. At this energy we need both components of the $I=0$ and $I=1$ exchange and both with attractive long-range and repulsive short-range potentials. Figure 3 presents a Fourier transform of the imaginary potential into configuration space illustrating these features of the potential shape.

At 970 MeV the imaginary potential leads to in-

TABLE II. Parameters of the imaginary potential.

| | 660 MeV | | 970 MeV | |
|---|---|---|---|---|
| | No. 1 | No. 2 | No. 1 | No. 2 |
| $(g_l^0)^2$ | 11.50 | 11.02 | 18.70 | 18.40 |
| $(g_h^0)^2$ | 31.82 | | 43.10 | |
| $(g_l^1)^2$ | 2.31 | | 0.00 | |
| $(g_h^1)^2$ | 8.16 | | 3.00 | |
| $\Lambda_l$ (MeV) | 1100.0 | | 1100.0 | |
| $\Lambda_h$ (MeV) | 1980.0 | | 1980.0 | |

elastic cross sections which are fairly good. To match the observed $l$ dependence of the reflection parameters our imaginary potential has been made to be of peripheral type. At this energy the $I=0$ exchange part dominates and the $I=1$ part is very small.

### D. Observables

To deal with the ambiguity of the phase-shift analysis solutions we have made direct comparisons with experimental observables at 660 and 970 MeV. In Fig. 4 we show the theoretical predictions of solutions 1 and 2 for the $pp$ and $np$ observables which are the differential cross section $d\sigma/d\Omega$ (mb/sr), polarization $P$, depolarization $D$, the spin rotations $R, A$, and the spin correlation parameters $C_{NN}, C_{KP}$ compared with the data.[28]

## 6. DISCUSSION AND CONCLUSION

### A. Comparison with Result of the Dispersion Relation Calculation

First we compare the present calculation with the result given by Ueda, using the dispersion relation with inelastic effects in the 0–3-GeV energy range.[10] Comparisons of the $^1S_0$, $^3P_{0,1,2}$, and $^1D_2$ phase shifts in the 0–1-GeV energy range show that both calculations give qualitatively similar results. However, an appreciable difference is noted in the $^1D_2$ phase parameter where the present one decreases with increase of energy more rapidly than that of the dispersion relation calculation in the 400–1000-MeV energy range.

The present calculation shows that the inelastic effect on the real phase shifts are not so large and in most cases makes the real phase shifts go downward, i.e., it acts repulsively. However, the dispersion relation calculation indicated that the inelastic effect on the real phase shifts are more appreciable and act attractively in the sub-GeV region, although at very high energy it acts repulsively. These basic differences must be resolved by future study.

### B. Energy Dependent Parameters of the Imaginary Potential

We have chosen the strength parameters $g_l$ and $g_h$ of the imaginary potential at each energy and

TABLE III. Real phase parameters ($\delta$ or $\epsilon$) in degrees for solutions 1 and 2 computed using $V = V_R + iV_I$ at 660 and 970 MeV compared with computation using only $V_R$ to show the quantitative effect of adding $V_I$ at these energies.

| | 660 MeV | | | | 970 MeV | | | |
|---|---|---|---|---|---|---|---|---|
| | No. 1 | | No. 2 | | No. 1 | | No. 2 | |
| $\delta$ or $\epsilon$ | $V$ | $V_R$ | $V$ | $V_R$ | $V$ | $V_R$ | $V$ | $V_R$ |
| $^1S_0$ | −38.9 | −37.1 | −41.9 | −39.7 | −57.6 | −56.1 | −61.0 | −58.9 |
| $^3P_0$ | −39.3 | −38.7 | −41.0 | −40.4 | −57.1 | −56.2 | −58.3 | −57.2 |
| $^1P_1$ | −34.4 | −22.3 | −38.6 | −35.8 | −31.9 | −3.9 | −41.9 | −36.7 |
| $^3S_1$ | −39.1 | −39.7 | −33.8 | −34.2 | −57.2 | −52.4 | −52.0 | −51.8 |
| $^3P_1$ | −41.0 | −40.5 | −39.1 | −38.7 | −49.3 | −48.8 | −46.8 | −46.6 |
| $^3D_1$ | 21.7 | 19.8 | 3.0 | 3.0 | 40.5 | 31.8 | 11.4 | 11.3 |
| $\epsilon_1$ | 4.7 | 6.5 | −1.9 | −1.5 | −1.7 | −1.4 | −4.7 | −6.3 |
| $^1D_2$ | 5.4 | 5.9 | 4.3 | 4.6 | −0.4 | −0.2 | −2.5 | −2.4 |
| $^3P_2$ | 11.4 | 14.8 | 10.5 | 13.6 | 5.0 | 9.1 | 3.1 | 6.5 |
| $^3D_2$ | 20.9 | 21.0 | 14.9 | 14.9 | 7.9 | 8.2 | 1.1 | 1.3 |
| $^3F_2$ | −5.7 | −5.6 | −6.9 | −6.8 | −14.3 | −14.3 | −16.0 | −16.0 |
| $\epsilon_2$ | 0.7 | 1.0 | 1.1 | 1.3 | 2.1 | 2.5 | 2.3 | 2.7 |
| $^1F_3$ | −9.5 | −9.5 | −10.2 | −10.1 | −15.5 | −15.3 | −16.5 | −16.2 |
| $^3D_3$ | 3.2 | 3.1 | 5.9 | 6.0 | −1.9 | −1.9 | 1.7 | 1.9 |
| $^3F_3$ | −8.1 | −7.9 | −8.3 | −8.1 | −12.0 | −11.7 | −12.4 | −12.1 |
| $^3G_3$ | −5.0 | −5.0 | −4.8 | −4.9 | 1.8 | 1.7 | 0.0 | −0.1 |
| $\epsilon_3$ | 7.2 | 7.7 | 5.9 | 6.2 | 4.6 | 5.2 | 3.2 | 3.1 |
| $^1G_4$ | 2.6 | 2.7 | 2.6 | 2.6 | 2.6 | 2.8 | 2.4 | 2.6 |
| $^3F_4$ | 3.8 | 4.0 | 3.6 | 3.8 | 3.1 | 3.6 | 2.6 | 3.0 |
| $^3G_4$ | 12.7 | 12.7 | 11.6 | 11.6 | 12.0 | 12.1 | 10.0 | 10.1 |
| $^3H_4$ | 0.7 | 0.7 | 0.5 | 0.5 | −0.7 | −0.7 | −1.3 | −1.3 |
| $\epsilon_4$ | −1.9 | −2.1 | −1.8 | −1.9 | −1.5 | −1.7 | −1.3 | −1.5 |
| $^1H_5$ | −2.4 | −2.4 | −2.5 | −2.5 | −3.5 | −3.5 | −3.9 | −3.8 |
| $^3G_5$ | 0.1 | 0.1 | 0.4 | 0.4 | −0.2 | 0.0 | 0.4 | 0.6 |
| $^3H_5$ | −2.1 | −2.1 | −2.1 | −2.1 | −3.0 | −3.0 | −3.1 | −3.1 |
| $^3I_5$ | −2.1 | −2.1 | −2.0 | −2.0 | −2.4 | −2.4 | −2.3 | −2.3 |
| $\epsilon_5$ | 4.6 | 4.6 | 4.4 | 4.5 | 4.9 | 5.2 | 4.6 | 4.9 |

TABLE IV. Reflection parameters $(\rho,r)$ for phase shifts $\delta$, and $(\alpha,\phi)$ for mixing parameters $\epsilon$ or $\rho$ as defined in our Appendix according to the (Livermore, Kyoto) definitions, respectively, and inelastic cross sections.

| | 660 MeV | | | | 970 MeV | | | |
|---|---|---|---|---|---|---|---|---|
| State | No. 1 $\rho$ (deg) | No. 2 $\rho$ (deg) | No. 1 $r$ | No. 2 $r$ | No. 1 $\rho$ (deg) | No. 2 $\rho$ (deg) | No. 1 $r$ | No. 2 $r$ |
| $^1S_0$ | 16.7 | 8.3 | 0.96 | 0.99 | 25.4 | 22.7 | 0.90 | 0.92 |
| $^3S_1$ | 31.1 | 24.5 | 0.86 | 0.91 | 133.6 | 141.4 | 0.69 | 0.79 |
| $^3P_0$ | 42.1 | 41.6 | 0.74 | 0.75 | 48.8 | 49.1 | 0.66 | 0.65 |
| $^1P_1$ | 34.9 | 29.0 | 0.82 | 0.88 | 63.4 | 56.7 | 0.45 | 0.55 |
| $^3P_1$ | 47.7 | 47.2 | 0.67 | 0.68 | 55.5 | 55.2 | 0.57 | 0.57 |
| $^3P_2$ | 8.8 | 5.8 | 0.99 | 0.99 | 8.1 | 15.6 | 0.99 | 0.96 |
| $^3D_1$ | 39.3 | 28.6 | 0.78 | 0.88 | 56.3 | 53.0 | 0.56 | 0.61 |
| $^1D_2$ | 42.9 | 41.3 | 0.73 | 0.75 | 50.1 | 48.7 | 0.64 | 0.66 |
| $^3D_2$ | 25.1 | 22.7 | 0.91 | 0.92 | 47.3 | 45.6 | 0.68 | 0.70 |
| $^3D_3$ | 28.5 | 27.3 | 0.89 | 0.89 | 54.2 | 54.1 | 0.60 | 0.59 |
| $^3F_2$ | 20.7 | 19.9 | 0.94 | 0.94 | 28.1 | 27.5 | 0.88 | 0.89 |
| $^1F_3$ | 14.0 | 13.1 | 0.97 | 0.97 | 33.7 | 33.3 | 0.83 | 08.4 |
| $^3F_3$ | 24.4 | 23.8 | 0.91 | 0.91 | 34.7 | 34.2 | 0.82 | 0.83 |
| $^3F_4$ | 30.9 | 30.2 | 0.86 | 0.86 | 42.5 | 41.8 | 0.74 | 0.75 |
| $^3G_3$ | 10.1 | 9.1 | 0.99 | 0.99 | 30.0 | 26.7 | 0.87 | 0.89 |
| $^1G_4$ | 16.1 | 15.8 | 0.96 | 0.96 | 26.0 | 25.6 | 0.90 | 0.90 |
| $^3G_4$ | 9.8 | 9.0 | 0.99 | 0.99 | 25.8 | 24.8 | 0.90 | 0.91 |
| $^3G_5$ | 10.3 | 9.8 | 0.98 | 0.99 | 28.8 | 28.9 | 0.88 | 0.88 |
| $^3H_4$ | 6.8 | 6.6 | 0.99 | 0.99 | 12.2 | 12.0 | 0.98 | 0.98 |
| $^1H_5$ | 4.4 | 4.1 | 1.00 | 1.00 | 14.3 | 14.1 | 0.97 | 0.97 |
| $^3H_5$ | 7.6 | 7.4 | 0.99 | 0.99 | 14.2 | 14.0 | 0.97 | 0.97 |
| $^3I_5$ | 2.1 | 2.0 | 1.00 | 1.00 | 7.8 | 7.7 | 0.99 | 0.99 |
| State | $\alpha$ (deg) = $\phi$ (deg) | | | | $\alpha$ (deg) = $\phi$ (deg) | | | |
| $^3S_1$-$^3D_1$ | −14.0 | 14.6 | | | −102.2 | −100.9 | | |
| $^3P_2$-$^3F_2$ | −3.4 | −3.6 | | | −4.4 | −2.9 | | |
| $^3D_3$-$^3G_3$ | −3.6 | −4.2 | | | −28.1 | −39.2 | | |
| $^3F_4$-$^3H_4$ | −2.0 | −2.2 | | | −7.8 | −8.6 | | |
| $^3G_5$-$^3I_5$ | −0.1 | −0.1 | Exp. | | −1.3 | −1.5 | Exp. | |
| $\sigma^{in}_{pp}$ (mb) | 19.4 | 18.3 | 18.5±1.1 | | 21.6 | 21.4 | 21.7±1.4 | |
| $\sigma^{in}_{np}$ (mb) | 16.2 | 14.3 | 13.6±3.2 | | 25.7 | 24.5 | 23.8±3.5 | |

found that the best values for the parameters differed at 660 and 970 MeV. The possibility of finding an imaginary potential which describes inelastic effects with a single analytic function (possibly smoothly energy-dependent) over the entire energy region of interest also remains for future study.

### C. Reflection Parameters

It is noted that the reflection parameter of unity is obtained for the $^1S_0$ state at 660 MeV, though the imaginary potential produces an appreciable effect on the real phase shift. This comes obviously from the following reason. The reflection parameter results from some averaging over the attractive part and repulsive part of the imaginary potential and can portend no effect from the imaginary potential. However, the effect of the imaginary potential on the real phase shift originates

TABLE V. The low-energy and deuteron parameters.

| | Solution 1 | Solution 2 | Ref. 16 | Experiment |
|---|---|---|---|---|
| $a_s$ (fm) | −25.45 | −25.05 | −23.68 | −23.72 [a] |
| $r_s$ (fm) | 2.65 | 2.68 | 2.51 | 2.73 [a] |
| $a_t$ (fm) | 5.50 | 5.21 | 5.40 | 5.41 [b] |
| $r_t$ (fm) | 1.87 | 1.82 | 1.79 | 1.71 [c] |
| $E_d$ (MeV) | 2.23 | 2.56 | 2.28 | 2.22 [d] |
| $Q$ (fm$^2$) [e] | 0.253 | 0.215 | 0.053 | 0.282 [d] |

[a] H. P. Noyes and H. M. Lipinski, Phys. Rev. C 4, 995 (1971).

[b] L. Koester and W. Nistler, Phys. Rev. Lett. 27, 956 (1971).

[c] H. P. Noyes, Phys. Rev. 130, 2025 (1963).

[d] R. Wilson, *The Nucleon-Nucleon Interaction* (Interscience, New York, 1963).

[e] Note that the units of $Q$ are fm$^2$, not fm$^{-2}$ as quoted in Refs. 31 and 15.

from some other type of averaging because of a complicated coupling between the real potential and imaginary potential. Therefore the reflection parameter of unity does not necessarily imply that the imaginary potential has no effect on the real phase shift.

### D. Mass Distributed Propagators of the $\pi$-$\pi$ System

It has been shown that the effect of the mass distribution of $\rho$ on the $N$-$N$ phase parameters can be approximately represented by a renormalization of the coupling constant[32,33] or an appropriate displacement of its mass from the observed mean value with the zero-width approximation.[12] In this paper the mass of $\rho$ was chosen to be 840 MeV rather than its usual mean value of 750 MeV in an effort to allow for its mass-distribution effect. The $\rho$ propagator corresponding to the actual mass distribution found from the $I=1$ $P$-wave $\pi$-$\pi$ phase shift and the one-pole approximation with 840 MeV are shown in Fig. 5. The comparison shows that this one-pole approximation is fairly good.

In Fig. 5 the $S^*$ propagator corresponding to the broad mass distribution $I=0$ $S$-wave $\pi$-$\pi$ phase-shift data is shown by the solid line. The composite propagator used in the present work which is constructed by the $\sigma_l$ and $\sigma_h$ contributions is shown by the dashed lines. In fitting the $N$-$N$ data the lighter mass component $\sigma_l$ requires a greater relative coupling constant than is expected from the $\pi$-$\pi$ data. Possibly this difference may be attributed to contribution from $I=0$, $L=0$ part of the uncorrelated two-pion exchange. This approximation of identifying the uncorrelated two-pion-exchange contribution with a fictitious low mass $I=0$ scalar-meson-exchange contribution in the elastic region has been suggested by Furuichi.[33]

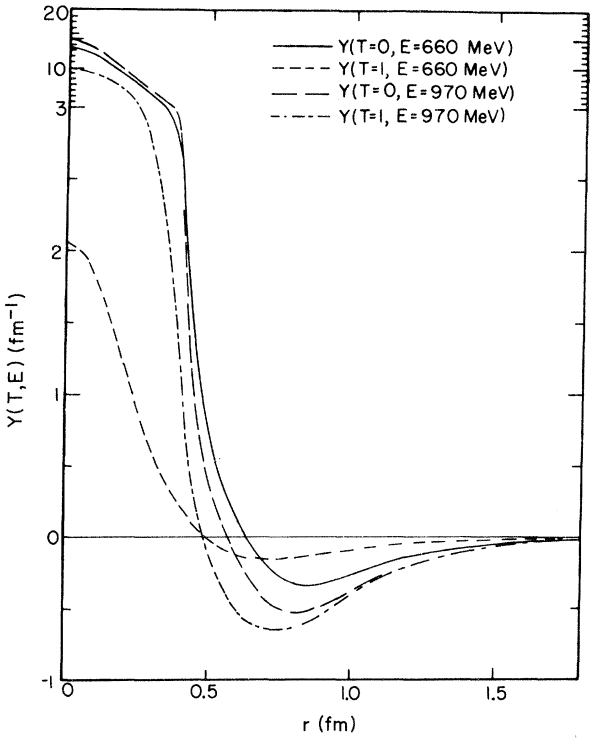


FIG. 3. Fourier transforms ($F$) or $x$ space potentials (see Ref. 3) of the $T=0$, 1 parts of Eq. (7), denoted symbolically by $Y(T=0, E)=F(v_0+v_1)$ and $Y(T=1, E)=F(v_0-3v_1)$, where $v_i$ are defined by Eq. (8). Only sol. 2 is shown at $E=660$, 970 MeV as sol. 1 only differs slightly in $g_1^0$. A (compressed, expanded) scale is used for ($Y>3$, $Y<3$), respectively, to best show the short- and long-range behavior.

### E. Form-Factor Parameters

Few of the particles listed in standard tables are elementary—i.e., specified only by the parameters of mass and conserved charges or quantum numbers. For example, resonances require at least a width parameter $\Gamma$, if not actually the more detailed phase-shift behavior.[12] It was noted by Ueda and Green[3] that the nucleon is not elementary, and that its virtual pion cloud structure can be represented by a form factor whose size and polarity parameters are ($\lambda=\hbar c/\Lambda$, $N$), respectively. The case $N=4$ of quadrupole regularization or a dipole nucleon-meson form factor results in an exponential pion density in $x$ space, and is used to fit the electromagnetic data as well as the strong interaction data of this paper. We see different $\lambda$'s depending on the interaction we use to probe the nucleon. The hadrons see the strong $\lambda_S^e=\hbar c/\Lambda=0.095$ fm of solution 1 of this work in the elastic region, and $\lambda_S^i=\hbar c/\Lambda_I=0.179$ fm in the inelastic region at 660 MeV. The larger size parameter at 660 MeV could reflect the excited nature of the nucleon $N^*$ at this energy. It is not surprising that the electromagnetic interaction probes the nucleon with a different size parameter $\lambda_{EM}=\hbar c/840$ MeV $=0.235$ fm, as it is a long-range force.

In final conclusion this work indicates that the generalized one-boson-exchange potential with an imaginary potential can describe the $N$-$N$ data in the 0–1-GeV energy range. It is especially noteworthy that our $^1S_0$ phase shift, which represents most sensitively the interaction in the innermost region, fits the phenomenological phase shifts over the entire energy range.

The authors would like to thank Dr. T. Sawada for useful conversations about the imaginary potential. One of us (T.U.) thanks Dr. A. Salam for his hospitality at the International Center for Theoretical Physics, Trieste. A final thanks goes to the North East Regional Data Processing Center at the University of Florida, Gainesville, for their computational support.

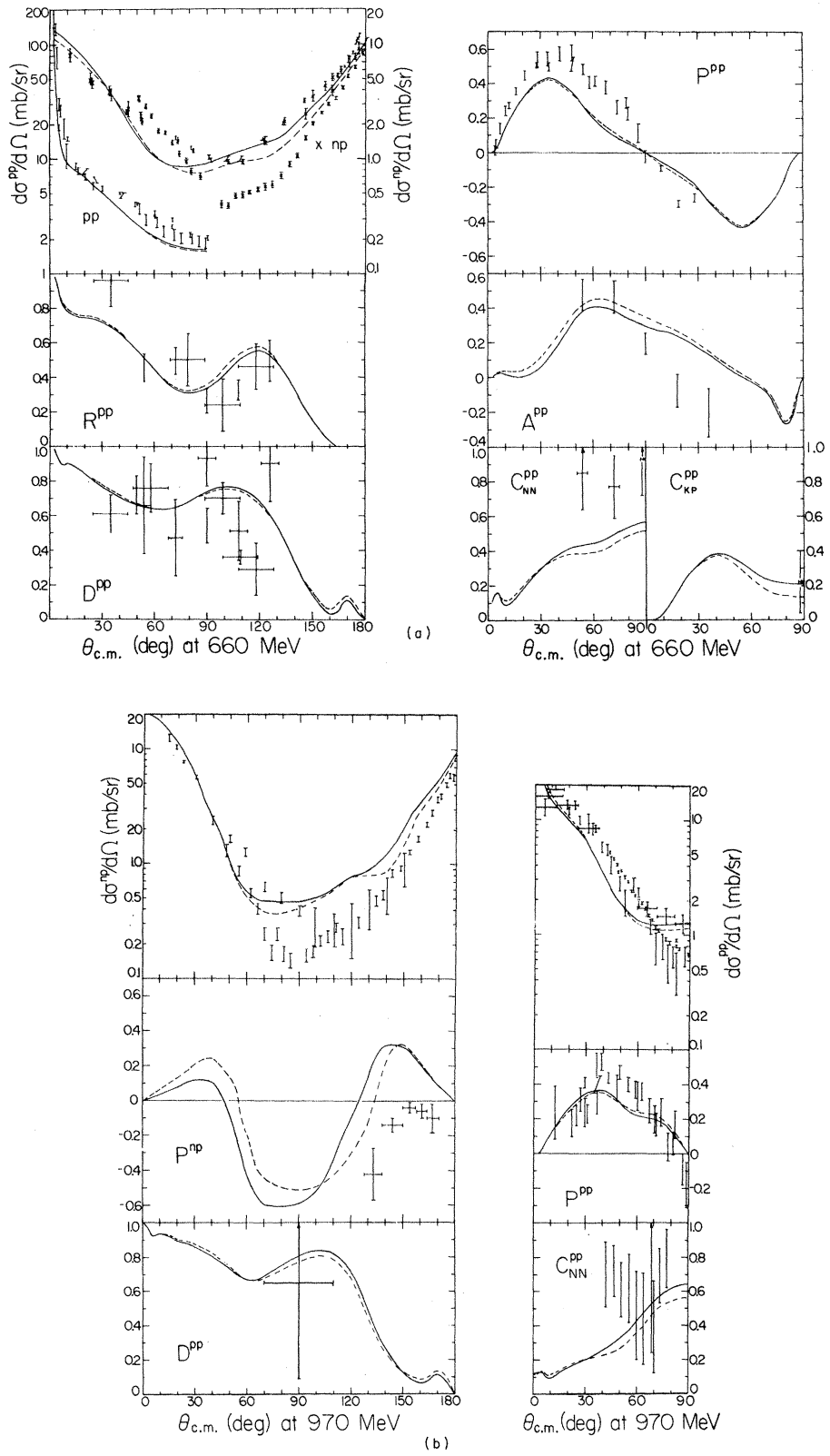


FIG. 4. Observables at (a) 660 MeV and (b) 970 MeV as predicted by sol. 1 (solid curve) and sol. 2 (broken curve).

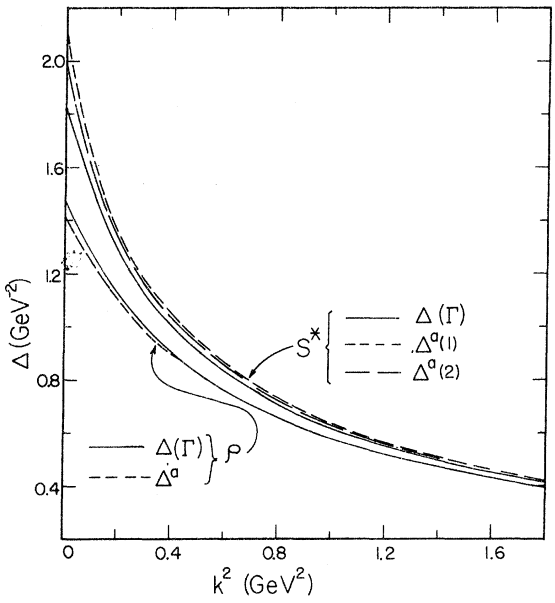


FIG. 5. The distributed $S^*$ and $\rho$ propagators $\Delta(\Gamma)$ (smooth curves) of Ref. 12 compared with their approximations $\Delta^a$ (dashed curves) used in this paper, where $\Delta(k^2, m^2) = (k^2 + m^2)^{-1}$, $\Delta(\Gamma) = \int \Delta(k^2, t')\rho^g(t')dt'$ for $t' = m'^2$, and $\rho^g(t')$ is the spectral function of the $S^*$ or $\rho$. The approximations are $\Delta^a = p\Delta(k^2, m_h^2) + (1-p)\Delta(k^2, m_l^2)$ for sols. 1 and 2 of the $S^*$ where $p = g^2(\sigma_h)/[g^2(\sigma_h) + g^2(\sigma_l)]$, $p = 1$ for the $\rho$, and $m_h \approx \bar{m}$ or the mean mass for both the $S^*$ and $\rho$ as determined from $\rho^g(t')$.

## APPENDIX

For the spin-coupled scattering with the inelastic effect we used the two following parametrizations of the $S$ matrix:

$$S = \begin{pmatrix} S_{J-1,J} & R^J \\ R^J & S_{J+1,J} \end{pmatrix}, \tag{A1}$$

where

$$S_{J\mp1,J} = [1 - (r_{J\pm1,J}/r_{J\mp1,J})\rho_J{}^2]^{1/2} r_{J\mp1,J} \exp(2i\delta_{J\mp1,J}), \tag{A2}$$

$$R^J = i\rho_J (r_{J-1,J} r_{J+1,J})^{1/2} \exp[i(\delta_{J-1,J} + \delta_{J+1,J} + \phi_J)], \tag{A3}$$

and

$$S = \begin{pmatrix} \cos\rho_- \cos 2\epsilon\, e^{2i\delta_-} & i\sin 2\epsilon\, e^{i(\delta_- + \delta_+ + \alpha)} \\ i\sin 2\epsilon\, e^{i(\delta_- + \delta_+ + \alpha)} & \cos\rho_+ \cos 2\epsilon\, e^{2i\delta_+} \end{pmatrix}. \tag{A4}$$

In these expressions the sign $\pm$ denotes a relation $l = J \pm 1$. Inelastic cross sections are related with the reflection parameters $r$ as follows:

$$\sigma_{p\bar{p}}^{\text{in}} = \frac{\pi}{2k^2}\left\{ \sum_{J:\text{even}} (2J+1)[1 - ({}^1r_J)^2] + \sum_{L:\text{odd}} \sum_{J=L-1}^{L+1} (2J+1)[1 - ({}^3r_{LJ})^2] \right\}, \tag{A5}$$

$$\sigma_{n\bar{p}}^{\text{in}} = \frac{\pi}{4k^2}\left\{ \sum_{J} (2J+1)[1 - ({}^1r_J)^2] + \sum_{L} \sum_{J=L-1}^{L+1} (2J+1)[1 - ({}^3r_{LJ})^2] \right\}, \tag{A6}$$

where $k$ is the c.m. momentum of any nucleon, and ${}^1r_J$ and ${}^3r_{LJ}$ represent the reflection parameters for the singlet and triplet scattering, respectively.

---


*On leave from Osaka University.

[1] T. Ueda, in Proceedings of the International Symposium on Present Status and Novel Developments in the Nuclear Many-Body Problem, Rome, 1972 (unpublished); S. Ogawa, S. Sawada, T. Ueda, W. Watari, and M. Yonezawa, Prog. Theor. Phys. Suppl. 39, 140 (1967).

[2] S. Sawada, T. Ueda, W. Watari, and M. Yonezawa, Prog. Theor. Phys. 28, 991 (1962); 32, 380 (1964).

[3] T. Ueda and A. E. S. Green, Phys. Rev. 174, 1304 (1968); Nucl. Phys. B10, 289 (1969).

[4] A. E. S. Green and T. Sawada, Nucl. Phys. B2, 276 (1967); Rev. Mod. Phys. 39, 594 (1967).

[5] A. E. S. Green, Phys. Rev. 73, 519 (1948).

[6] A. Gersten, R. H. Thompson, and A. E. S. Green, Phys. Rev. D 3, 2076 (1971); D 3, 2069 (1971).

[7] E. E. Salpeter and H. A. Bethe, Phys. Rev. 84, 1232 (1951); R. Blankenbecler, and R. Sugar, Phys. Rev. 142, 1051 (1966).

[8] M. Kikugawa, T. Ueda, S. Sawada, W. Watari, and M. Yonezawa, Prog. Theor. Phys. 37, 88 (1967).

[9] M. Kikugawa, W. Watari, and M. Yonezawa, Prog. Theor. Phys. 43, 407 (1970).

[10] T. Ueda, Prog. Theor. Phys. 45, 1527 (1971); Phys. Rev. Lett. 26, 588 (1971).

[11] R. H. Thompson, Phys. Rev. D 1, 110 (1970).

[12] M. L. Nack, T. Ueda, and A. E. S. Green, to be published.

[13] T. Ueda, Prog. Theor. Phys. 48, 2276 (1972).

[14] S. Furuichi, H. Suemitsu, M. Yonezawa, and W. Watari, to be published.

[15] R. A. Bryan and A. Gersten, Phys. Rev. D 6, 341

(1972).
[16]M. H. MacGregor, R. A. Arndt, and R. M. Wright, Phys. Rev. 182, 1714 (1969); 169, 1149 (1968); 173, 1272 (1968).
[17](a) N. Hozhizaki, Prog. Theor. Phys. Suppl. 42, 1 (1968); (b) N. Hoshizaki and T. Kadota, Prog. Theor. Phys. 42, 815 (1969).
[18]U. Amaldi, Rev. Mod. Phys. 39, 649 (1967).
[19]R. E. Seamon, K. A. Friedman, G. Breit, R. D. Haracz, J. M. Holt, and A. Prakash, Phys. Rev. 165, 1579 (1968).
[20]S. Mandelstam, Proc. R. Soc. Lond. A244, 491 (1958).
[21]D. V. Bugg, D. C. Salter, G. H. Stafford, R. F. George, K. F. Riley, and R. J. Tapper, Phys. Rev. 146, 980 (1966).
[22]N. S. Amaglobeli and Yu. M. Kazarinov, Zh. Eksp. Teor. Fiz. 37, 1587 (1959) [transl.: Sov. Phys.—JETP 37, 1125 (1960)].
[23]A. P. Batson, B. B. Culwick, H. B. Klepp, and L. Riddiford, Proc. R. Soc. Lond. A251, 233 (1959).
[24]T. A. Murray, L. Riddiford, G. H. Grayer, T. W. Jones, and Y. Tanimura, Nuovo Cimento 49A, 261 (1967).
[25]N. P. Bogachev, Dokl. Akad. Nauk. USSR 108, 806 (1956) [transl.: Sov. Phys.—Dokl. 1, 361 (1956)].
[26]D. V. Bugg, A. J. Oxley, J. A. Zoll, J. G. Rushbrooke, V. E. Barnes, J. B. Kinson, W. P. Dodd, G. A. Doran, and L. Riddiford, Phys. Rev. 133, B1017 (1964).
[27]N. Hoshizaki, Prog. Theor. Phys. Suppl. 42, 107 (1968).
[28]J. Bystricky, F. Lehar, and Z. Janout, *Elastic Nucleon-Nucleon Scattering Data 270-3000 MeV* (Centre d'Etudes Nucléaires de Saclay, 1972): A-3, 9, 17; B-11, 13,14, 15, 25, 27, 93; C-26; D-31; G-5, 6, 21; H-24; J-7; K-10, 12, 14, 15; L-6; M-16, 31, 33; N-3, 6, 9; R-9, 13, 15; S-9, 12; W-7.
[29]R. Tamagaki, M. Wada, and W. Watari, Prog. Theor. Phys. 31, 623 (1964).
[30]Y. Kishi, S. Sawada, and W. Watari, Prog. Theor. Phys. 38, 892 (1967).
[31]A. Gersten and A. E. S. Green, Phys. Rev. 176, 1199 (1968).
[32]S. Furuichi, S. Sawada, T. Ueda, M. Yonezawa, and W. Watari, Prog. Theor. Phys. 32, 966 (1964).
[33]S. Furuichi, Prog. Theor. Phys. Suppl. 39, 190 (1967).